III

High light

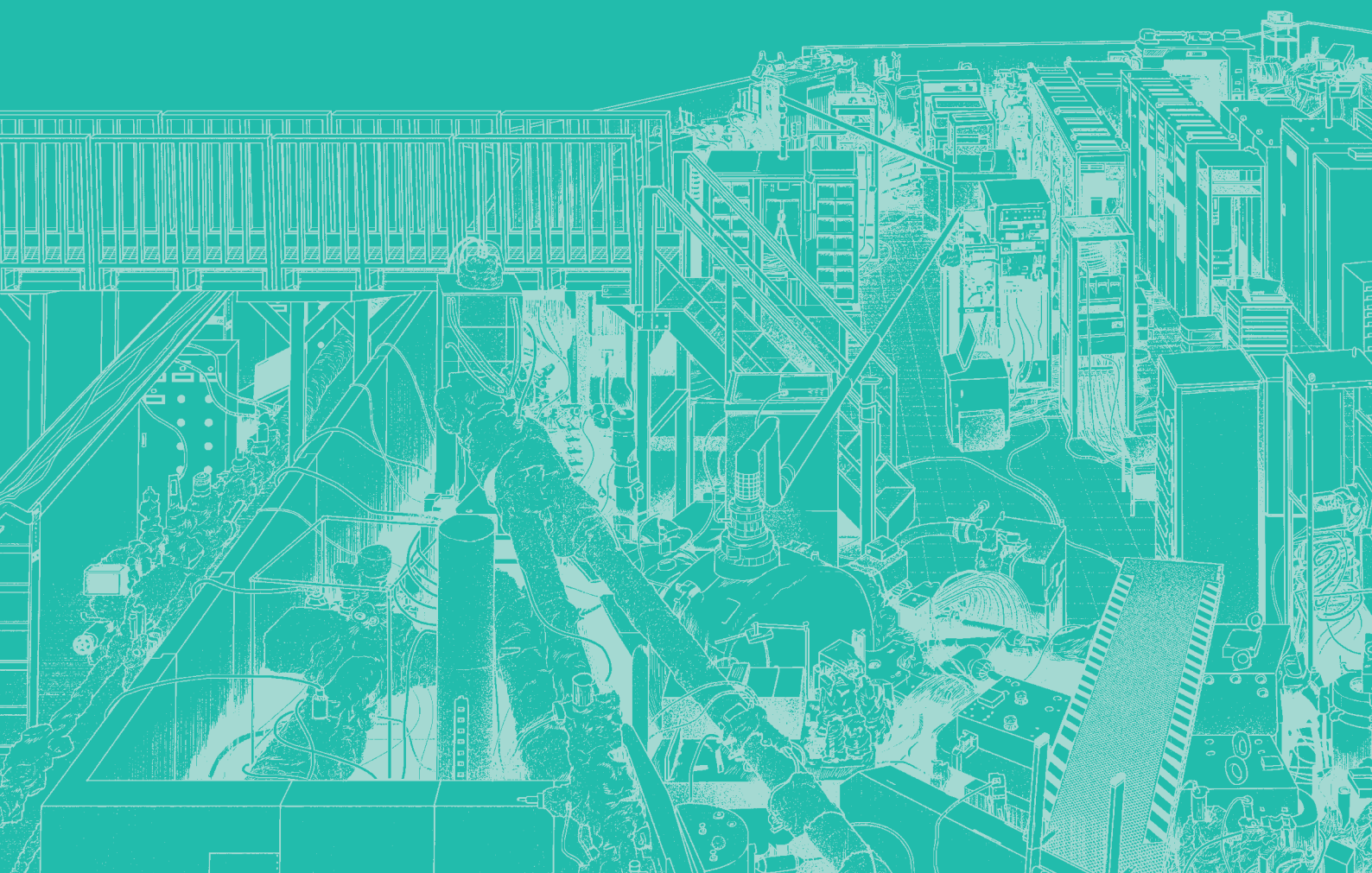

BL1U

Change in Positron Lifetime of Tensile-Deformed Pure Iron after Stress Release and Room-Temperature Aging

M. Fujinami[1], R. Awaji[1], H. Abe[1], A. Yabuuchi[2], T. Hirade[3], N. Oshima[4] and Y. Taira[5]

[1]*Department of Applied Chemistry and Biotechnology, Chiba University, Chiba 263-8522, Japan*
[2]*Institute for Integrated Radiation and Nuclear Science, Kyoto University, Kumatori 590-0494, Japan*
[3]*Nuclear Science and Engineering Center, Japan Atomic Energy Agency, Tokai 319-1195, Japan*
[4]*National Institute of Advanced Industrial Science and Technology, Tsukuba 305-8568, Japan*
[5]*UVSOR Synchrotron Facility, Institute for Molecular Science, Okazaki 444-8585, Japan*

Understanding the formation of lattice defects in metals not only while applying deformation stress but also after releasing stress and subsequent aging is essential for accurately assessing the durability of structural materials. Positron annihilation lifetime spectroscopy (PALS) is an effective technique for examining vacancy-type defects within crystalline materials [1]. Nevertheless, measuring the positron lifetime in metals while applying deformation stress presents significant challenges when using conventional PALS techniques. As a result, most previous studies have conducted positron lifetime measurements on deformed metals only after the deformation stress has been released. It should be noted that the properties of defects within metals may undergo alterations when the deformation stress is released. This study applied PALS to a pure iron specimen subjected to tensile deformation, using the gamma-ray-induced PALS (GiPALS) technique [2].

A well-annealed pure iron specimen (99.99% purity) was elongated to ~7% nominal strain using a small tensile tester installed at the BL1U beamline (Fig. 1). The thickness and gauge width of the test piece were 3 mm and 6 mm, respectively. Positron lifetime measurements were conducted at three different stages following the deformation: (1) under applied stress after elongation, (2) after releasing the tensile stress, and (3) after 3 days at room temperature following the stress release. The results revealed significant changes in the longer positron lifetime component (associated with defect species) across the three conditions. In addition, the intensity of the defect component (I_2) changed from approximately 45% under stress to 60% immediately after unloading, and then decreased to 28% after 3 days of room-temperature aging (Fig. 2).

These findings suggest that tensile stress release leads to additional defect formation, while subsequent room temperature aging facilitates partial defect recovery. Therefore, it is essential to consider both stress release effects and room-temperature aging when characterizing defect structures in deformed metals. This highlights the importance of in situ characterization in studies of deformed structural materials.

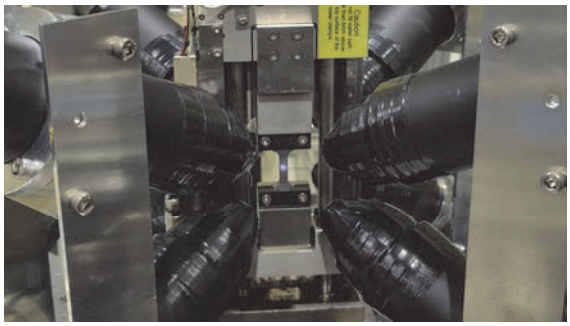

Fig. 1. A view of a small tensile tester installed at the BL1U beamline with a tensile test piece attached.

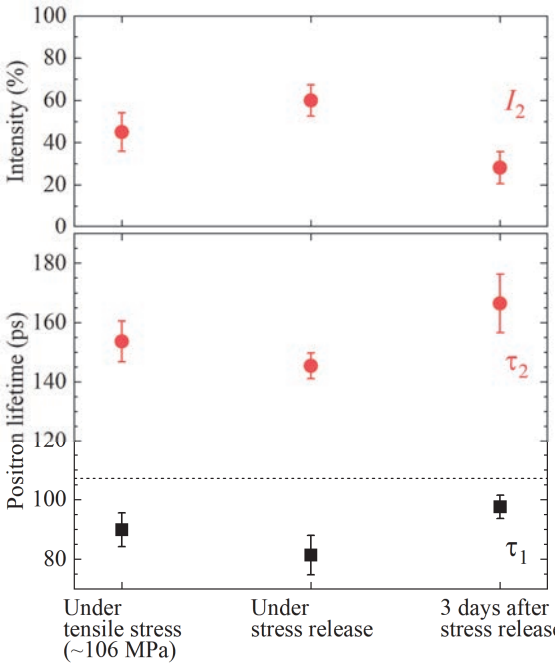

Fig. 2. Positron lifetimes and their intensities of elongated pure iron. The results are shown for the same specimen while applying stress, after releasing the stress, and after aging at room temperature for 3 days. The positron lifetime of the specimen before elongation is also depicted by the dashed line.

[1] R. W. Siegel, Annu. Rev. Mater. Sci. **10** (1980) 393.
[2] Y. Taira *et al.*, Rev. Sci. Instrum. **93** (2022) 113304.

BL3U

X-ray Absorption Spectra of Lipid Bilayer Membranes in Electrolyte Solutions and Its Dependence on Cation Species

R. Tero [1], Yu Kinjo[1] and M. Nagasaka[2]
[1]*Toyohashi University of Technology, Toyohashi 441-8580, Japan*
[2]*Institute for Molecular Science, Okazaki 444-8585, Japan*

The lipid bilayer is a self-assembled structure of amphiphilic lipid molecules. It is the fundamental structure of biomembranes such as cell membranes, which are the fields for the transportation of materials, information, and energy into and out of cells. All these physiological reactions proceed in the presence of electrolytes. Ions in the aqueous solution significantly influence physical properties and structures of lipid bilayers. Phosphatidylcholine (PC) is the most abundant lipid of eukaryotic cell membranes. Cations bind to the phosphate and carbonyl groups of PC. However, the affinity of cations to PC and effects of cations to molecular orientation are still controversy especially in the fields of theoretical simulations. We aim to determine the binding affinity of cations to lipids in aqueous solutions experimentally, by means of X-ray absorption spectroscopy (XAS) [1]. Recently, we measured the dependence of O-K edge XAS spectra of DOPC bilayer on Na^+ concentration in the aqueous solution [2, 3].

Supported lipid bilayers (SLBs) of dioleoyl-PC (DOPC) were formed on the Si_3N_4 membranes of the XAS flow cell [1] by the vesicle fusion method in a buffer solution (KCl 100 mM, HEPES 25 mM/ pH 7.4 KOH). The K^+ concentration ($[K^+]$) was varied by exchanging the buffer solution in the flow cell in in the range of $[K^+]$ = 2.1 – 510.4 mM. The O-K edge XAS spectra of SLB were obtained at the energy range of 527 – 535 eV. The X-ray incident angle of 35º. The XAS spectrum of the Si_3N_4 membrane without SLB was subtracted from that with SLB.

The O-K-edge spectrum of DOPC appeared at 531 - 533 eV [2, 3]. It consists of 1s→π* transitions of double-bond oxygens in the phosphate and carbonyl groups on the PC headgroup: two components attributed to the P=O in the former, and one component attributed to the latter. We measured XAS spectra at the X-ray incident angle (T) of 35º. We obtained a specific dependence of the P=O peak at the lower energy on $[K^+]$: its position was little affected by $[Na^+]$ in the range of 2.1 – 10.4 mM and shifted to higher energy by ~0.4 eV at $[K^+]$ = 20.4 mM, while the position showed slight change at $[K^+] \geq 50.4$ mM. The former tendency at was similar to that of Na^+ at $[Na^+] \leq 20.4$ mM, but latter was different from the peak shift and broadening observed at $[Na^+] \geq 50.4$ mM [2, 3].

The inner-shell quantum chemical calculation [4] of O K-edge spectrum of P=O indicated that coordination of K^+ to the phosphate group causes higher-energy shift of P=O peaks. The XAS spectra shows the difference in the coordination affinity between K^+ and Na^+. The effects of the cation species on the XAS components will be evaluated by the theoretical calculations.

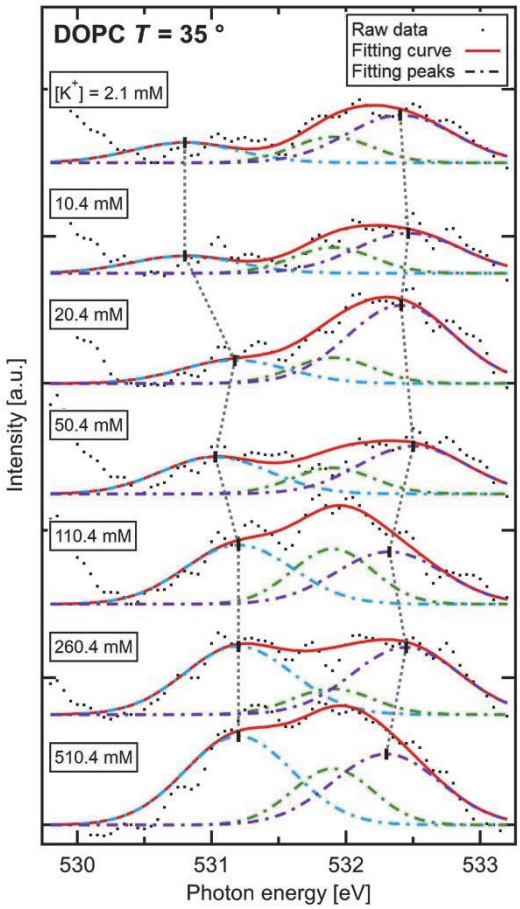

Fig. 1. O K-edge XAS spectra of DOPC-SLB at $[K^+]$ = 2.1 – 510.4 mM obtained at the X-ray incident angle of 35°. Black dotted curves represent raw data. Dashed curves and red solid curves show deconvoluted components and their summation, respectively.

[1] M. Nagasaka *et al.* , J. Electron Spectros. Relat. Phenomena **224** (2018) 93.
[2] R. Tero, Y. Kinjo and M. Nagasaka, UVSOR Activity Report **50** (2022) 165.
[3] R. Tero, W.-Z. Goh and M. Nagasaka, UVSOR Activity Report **51** (2023) 174.

BL3B, 6B

Temperature-Dependent Electronic Structure Modification on an Altermagnet Candidate MnTe

S. Kimura[1,2,3], H. Watanabe[1,2], K. Yuan[2], Y. Pan[2], H. Ishida[2] and M.-H. Jung[4]
[1]*Graduate School of Frontier Biosciences, The University of Osaka, Suita 565-0871, Japan*
[2]*Department of Physics, Graduate School of Science, The University of Osaka, Toyonaka 560-0043, Japan*
[3]*Institute for Molecular Science, Okazaki 444-8585, Japan*
[4]*Department of Physics, Sogang University, Seoul 04107, Republic of Korea*

Recently, materials with antiferromagnetic and ferromagnetic characters, namely altermagnet, have attracted attention and are classified as the third magnetic material group [1]. The materials have no net magnetism, but owing to the crystal symmetry combined with the antiferromagnetic structure, there are two novel characteristics: a strong time-reversal symmetry-breaking response and the other spin-polarization phenomena typical of ferromagnets [2]. Thanks to their physical properties, the materials are considered helpful for spintronics devices [3].

One candidate for altermagnets is MnTe. The material has a Neel temperature of 307 K. The Spin-split band structure of the material has been observed with angle-resolved photoelectron spectroscopy (ARPES) [4, 5]. The experimental result is considered to be evidence of the altermagnet.

ARPES can detect the occupied electronic structure below the Fermi level (E_F), but it is impossible to observe the unoccupied state. Thus, the whole band picture cannot be probed by ARPES. On the other hand, optical conductivity (σ_1) spectra have information on the joint density of states between the occupied and unoccupied states. By the experimental characters, the combination of ARPES and σ_1 spectra provides information on the unoccupied states. Additionally, in-gap states with very low density can be observed with σ_1 spectra. Then, we measured σ_1 spectra of MnTe.

Reflection spectroscopy has been performed at BL3B from the visible to the VUV regions and at BL6B from the IR to the THz regions. The measurements were combined with the reflection spectra in the IR – visible region taken at the laboratory, and finally, whole reflectivity spectra in the photon energy of 8 meV – 40 eV were obtained. σ_1 spectra were obtained with the Kramers-Kronig analysis of the wide-range reflectivity spectra.

Figure 1 shows the temperature dependence of the σ_1 spectrum of MnTe near the energy gap at 1 eV. At 370 K, higher than T_N, a broad peak is visible at about 2.25 eV. As the temperature decreases, the peak shifts to the low energy side and narrows. The temperature dependence is almost consistent with a valence band peak observed in ARPES results [5]. However, the energy shift is about 0.2 eV, much smaller than the peak shift of 0.4 eV appearing in ARPES. To clarify the inconsistency, further band structure calculations are needed.

As shown in the inset of Fig. 1, the structural temperature change within the energy gap appearing at the low energy side is remarkable. With decreasing temperature, the intensity at around 0.5 eV decreases, while that below 0.2 eV increases. The former corresponds to the onset of the absorption edge shifting to the high energy side, which is the opposite behavior of the peak energy. This suggests that the band structure at the gap edge is modulated with decreasing temperature. The newly appeared peak below 0.2 eV suggests another localized electronic state emerges in the energy gap below T_N.

The observed characteristic temperature dependence in the σ_1 spectrum does not correspond to conventional antiferromagnetic materials; the spectral change can be regarded as originating from the band modification of altermagnetic character.

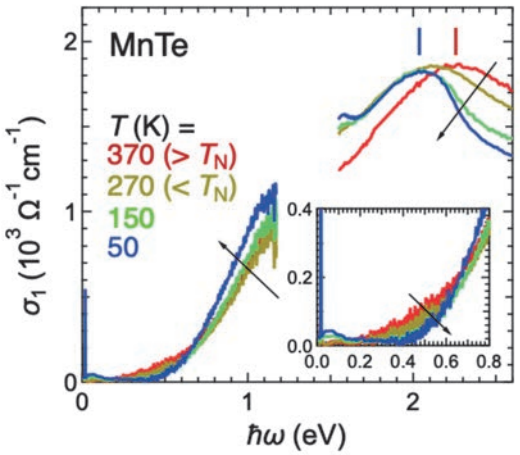

Fig. 1. Temperature-dependent optical conductivity [σ_1] spectra of MnTe near the energy gap. (Inset) The enlarged figure of the in-gap states.

[1] I. Mazin, Phys. Rev. X **12** (2022) 040002.
[2] L. Šmejkal, J. Sinova and T. Jungwirth, Phys. Rev. X **12** (2022) 040501.
[3] C. Sun and J. Linder, Phys. Rev. B **108** (2023) L140408.
[4] S. Lee *et al.*, Phys. Rev. Lett. **132** (2024) 036702.
[5] T. Osumi *et al.*, Phys. Rev. B **109** (2024) 115102.

BL4U

Carbon K-Edge NEXAFS and Sulfur L-Edge NEXAFS Measurements of Samples from Asteroid Ryugu

T. Matsumoto[1]

[1]*The Hakubi Center for Advanced Research, Kyoto University Kitashirakawa-Oiwakecho, Sakyo, Kyoto 606-8502, Japan*

The *Hayabusa2* spacecraft from the Japan Aerospace Exploration Agency (JAXA) explored the asteroid Ryugu and returned surface grains to Earth. It was anticipated that the grains brought back directly from the asteroid might contain previously undiscovered substances not found in meteorites. Among these could be highly water-soluble materials, which readily react with moisture in Earth's atmosphere and are therefore difficult to detect unless examined in their pristine state as preserved in space.

In this study, Ryugu grains were analyzed using FE-SEM and (scanning) transmission electron microscopy ((S)TEM), and synchrotron radiation-based Scanning transmission X-ray microscopy (STXM). Thin sections for STXM and TEM analysis were prepared using a focused ion beam system (FIB). Near edge X- ray absorption fine structure (NEXAFS) spectra at carbon K-edge and sulfur L-edge of FIB sections of Ryugu grain C0071 were measured using the STXM beamline, BL4U. The custom-built sample transfer vessel and a nitrogen-filled glove box were used to prevent sample exposure to the air. The date analysis was performed using the aXis 2000 software.

Using a transmission electron microscope (TEM), which allows observation of structures at the nanometer scale, I identified sodium carbonates (Na_2CO_3 and a hydrate phase), halite crystals (NaCl: sodium chloride) in Ryugu grains. These mineral phases have not been reported in Ryugu samples. The STXM analyses were performed to identify chemical features of these sodium carbonates.

The C K-edge NEXAFS spectrum from the sodium carbonates exhibits a sharp peak at 290.2 eV, which is assigned to the 1s → π transition of carbonate (Fig. 1). Sulfur L-edge in the sodium carbonates of the grain C0071 corresponds to sodium sulfate (Fig. 1). STEM-energy dispersive X-ray spectrometer (EDX) analysis showed that the major elements within the sodium carbonates are sodium (Na), carbon (C), oxygen (O), with minor amounts of sulfur (S) (<6 atomic %) and fluorine (F) (<4 atomic %). STXM analysis suggests that sulfur component detected by STEM-EDS analysis is derived from sodium sulfate included in the sodium carbonate minerals.

The sodium salt minerals are all highly water-soluble. The fact that they dissolve easily in water suggests that their crystallization could only occur if the liquid was extremely limited and had a very high salt concentration. The salt minerals were hypothesized to be formed during the disappearance of the liquid water after the major aqueous minerals found in the Ryugu samples precipitated in the parent body. One possible explanation for the loss of liquid is the evaporation of saltwater. If large-scale fractures formed and connected the interior of the parent body to the outer vacuum environment, the liquid body could have undergone depressurization and evaporation. On Earth, when lakes dry up, highly concentrated saltwater forms, leading to the precipitation of minerals such as sodium carbonate and halite. The remnants of the vaporization are referred to as "evaporites". Similar processes may have occurred in Ryugu's parent body. Another possibility is the freezing of liquid water. After the Ryugu's parent body reached its peak temperature, it cooled due to the exhaustion of the radioactive heat. The remaining alkaline brines probably concentrated as H_2O ices formed. As a result, the sodium salts would have formed at subzero Celsius temperatures. The frozen ice could have sublimated into space over time. Currently, Ryugu shows no signs of large amounts of liquid, nor do its surface grains appear wet. Until now, it was unclear how the liquid water in the parent body was lost. This study has revealed that the loss of liquid water in Ryugu's parent body occurred through evaporation or freezing.

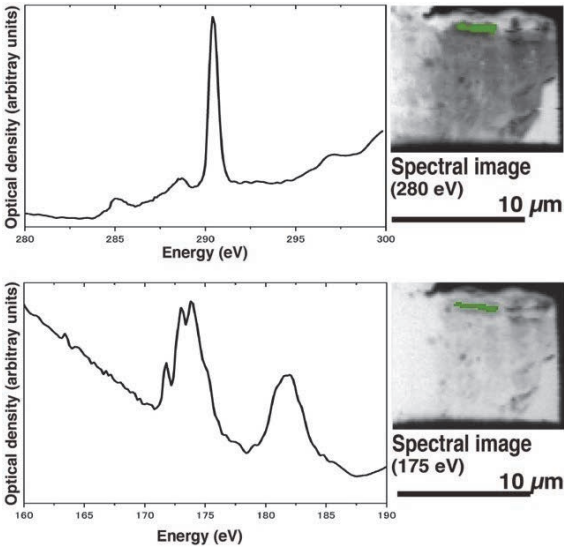

Fig. 1. The C K-edge NEXAFS spectrum (upper figure) and S L-edge NEXAFS spectrum of Ryugu sample(C0071).

[1] T. Mastsumoto *et al.*, *Nature Astronomy*, 8:12, 1536-1543. (2024)

BL4B

Collective Auger Decay of Double Inner-Shell Vacancies in Xe Studied by Multielectron–Ion Coincidence Spectroscopy

Y. Hikosaka[1]

[1]*Institute of Liberal Arts and Sciences, University of Toyama, Toyama 930-0194, Japan*

Auger decay of atomic and molecular core holes generally involves two-electron transitions, where an electron fills an inner-shell vacancy, causing another electron to be emitted into the continuum. An uncommon Auger process, called cascade Auger decay (CAD), can occur when double inner-shell vacancies form in atoms and molecules. Here, two outer electrons simultaneously fill the double vacancies while releasing a single high-energy Auger electron. This study investigates the CAD of Xe^{2+} $4d^{-2}$ double core-hole states using multielectron–ion coincidence spectroscopy with a magnetic bottle electron spectrometer [1,2]. Its high coincidence efficiency allows a detailed spectroscopic analysis of the very rare decay path of double core-hole states.

Figure 1(a) presents an Auger spectrum coincident with a $3d_{5/2}$ photoelectron, measured at a photon energy of 921.2 eV. The formation of $4d^{-2}$ double core-hole states is most prominent among the first-step Auger transitions from the $3d_{5/2}^{-1}$ state. The yields recorded in further coincidence with Xe^{3+} and Xe^{4+} are shown in red and blue, respectively, with ion detection efficiency being compensated. The decay of the double core-hole states mainly results in the production of Xe^{4+} due to cascade double Auger decay. Meanwhile, the red spectrum manifests that the decay of the $4d^{-2}$ states weakly produces Xe^{3+} through the emission of a single Auger electron, indicating a CAD path.

The Xe^{3+} levels populated by the CAD are distinctly observable in the single Auger electron spectrum emitted from the $4d^{-2}$ states. The Auger electron should be detected in a four-fold coincidence with a 3d photoelectron, an $M_{4,5}N_{4,5}N_{4,5}$ Auger electron, and a Xe^{3+} ion. The single Auger electron spectrum extracted is shown in Fig. 1(b), where the Auger transition energies from Xe^{2+} $4d^{-2}$ to Xe^{3+} $5l^{-3}$ levels and the energy position of the Xe^{4+} threshold relative to Xe^{2+} $4d^{-2}$ are indicated. The spectrum exhibits a broad structure in the kinetic energy range of 45–100 eV, suggesting that excited Xe^{3+} levels up to the Xe^{4+} threshold are predominantly produced by the CAD. This spectral feature differs significantly from the CAD observation for Ar^{2+} $2p^{-2}$, where Ar^{3+} $3p^{-3}$ ground states are mainly produced [3].

Peculiar behavior in the CAD of Xe^{2+} $4d^{-2}$ levels is observed also in the branching ratio relative to the total decay of the double core-hole states. The branching ratio is estimated from the coincidence yields to be as large as $2 \times 10^{-2} \pm 1 \times 10^{-2}$. The CAD branching ratio for Ar^{2+} $2p^{-2}$ states was reported to be $1.9 \times 10^{-3} \pm 1.0 \times 10^{-3}$ experimentally and approximately 1.0×10^{-3} theoretically [3]. Thus, the CAD branching ratio for Xe^{2+} $4d^{-2}$ double core-hole states is an order of magnitude greater than that for Ar^{2+} $2p^{-2}$. This amplified CAD for Xe^{2+} $4d^{-2}$, along with the favorable formation of excited Xe^{3+} levels, can be explained by analyzing the number and locations of intermediate configurations needed to promote CAD in second-order perturbation theory [4].

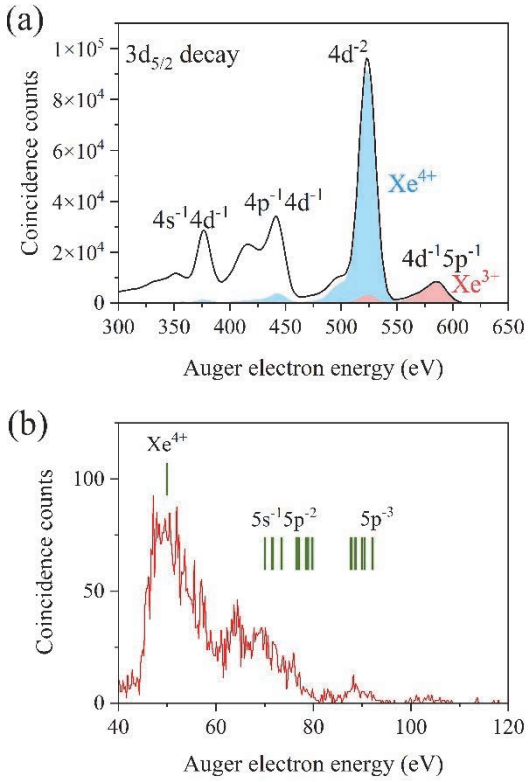

Fig. 1. (a) Coincident Auger spectrum (black) associated with the $3d_{5/2}$ core-hole state of Xe. The yield of Auger electrons, filtered further in coincidence with the Xe^{3+} and Xe^{4+} product ions, are shown in red and blue shading, respectively. (b) Spectrum of single Auger electrons emitted from the Xe^{2+} $4d^{-2}$ states populated via the decay of the $3d_{5/2}$ single vacancy levels, obtained through four-fold coincidence with a 3d photoelectron, an $M_{4,5}N_{4,5}N_{4,5}$ Auger electron, and a Xe^{3+} ion.

[1] Y. Hikosaka and E. Shigemasa, Int. J. Mass Spectrom. **439** (2019) 13.
[2] Y, Hikosaka, J. Electron Spectrosc. Relat. Phenom. **255** (2022) 147158.
[3] M. Mailhiot *et al*., Phys. Rev. A **107** (2023) 063108.
[4] Y. Hikosaka and S. Fritzsche, Phys. Rev. Lett. **134** (2025) 103001.

BL6B

Performance Evaluation of Infrared Microspectroscopy Station Using Human Hair

Y. Ikemoto[1] and T. Moriwaki[1]

[1]*Spectroscopy Divison, Japan Synchrotron Radiation Research Institute, Sayo, Hyogo 679-5198, Japan*

III

At infrared beamline BL43IR in SPring-8, microspectroscopy experiments under various sample environments have been conducted and many results have been published. Currently, SPring-8 upgrade plan is ongoing. After the upgrade, it will be difficult to obtain infrared beam due to a ring design. Therefore, it has been decided that BL43IR will be shut down in FY2025.

On the other hand, there is a high demand for research using infrared synchrotron radiation. On September 20, 2023, we held the UVSOR/SPring-8 Infrared Beamline Joint Users' Meeting, where we introduced the UVSOR infrared beamline BL6B to users of BL43IR/SPring-8. BL6B has maintained high performance of light source through facility upgrades. It was decided to start preparations for the transfer of SPring-8/BL43IR activities to BL6B at UVSOR. For the transfer, we must identify the necessary equipment to conduct experiments equivalent to those being conducted at BL43IR. In this proposal, human hair samples were measured, which have been measured at BL43IR as test samples to evaluate the spatial resolution and signal-to-noise ratio.

The sliced hair sample was put on a BaF_2 substrate (10 mm diameter, 1mm thickness) and placed on a sample stage of an infrared microscope (JASCO FT/IR-6100, IRT-7000) installed at BL6B. The absorption spectrum and its imaging were measured in the transmission configuration. The hair should be thin enough to prevent saturation of the absorption peak, which is known to be around 10 μm based on our experience, and we bring samples prepared to the appropriate thickness. The magnification of the objective mirror was x32. All measurements were performed at room temperature. Wavenumber resolution was 4 cm^{-1} and the wavenumber range is 8000-700 cm^{-1}, and a Ge/KBr beam splitter is used.

The following parameters will be varied to obtain a comparison data.

- Light source: standard light source inside the instrument, synchrotron radiation (SR)
- Measurement mode: imaging measurement using linear array detector, multi-point measurement using single element detector

In addition, a sliced hair sample were measured at the micorospectoroscopy station (BRUKER VERTEX70 and HYPERION2000) in BL43IR/SPring-8 for comparison. Wavenumber resolution, wavenumber range and beam splitter were the same as those in BL6B. Result are shown in Fig. 1. All data are mapping image, in which integrated C-H stretching band (2805 – 3141 cm^{-1}) intensity is plotted. The white bars in the figure correspond 20 μm. The samples are not exactly same but prepared at same condition and the thickness is almost same. Figure 1 (a) was measured at BL6B with standard light and 125 μm x 15 μm aperture. The detector was a linear array MCT detector. Figure 1 (b) was a result of BL6B with SR and 4 μm x 4 μm aperture. The detector was a single MCT element detector. Figure 1 (c) was measured at BL6B with SR and 125 μm x 15 μm aperture. The detector was a linear array MCT detector. Figure 1 (d) was measured at BL43IR/SPring-8 using SR with an aperture 5 μm x 5 μm. The detector was a single MCT element detector. Measurement times were 140 min, 220 min, 13min and 13 min for Fig. 1. (a) to (d), respectively. All image has lipid area called cortices are observed in the center. The size of the cortex is about 5 μm, and spatial resolutions are found to be smaller than that. In Fig. 1. (c), un-uniformity is observed, which is caused by non-uniform exposure of light to the array elements. It means that the SR spot is too small to the array detector. Measurement time is very short when array detectors are used. We propose a method at BL6B to measure a large number of samples with an array detector + standard light source, and to measure important samples over time with a single detector + SR. We will examine devices to control the sample environment such as humidification and temperature, and make preparations so that many users can continue their research at BL6B.

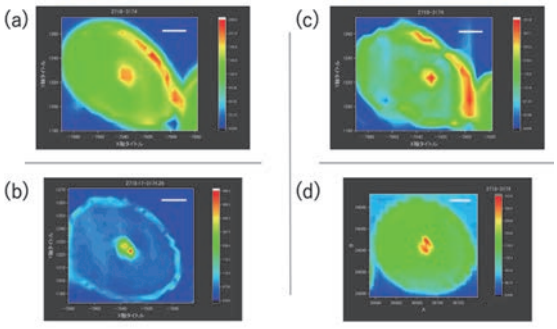

Fig. 1. CH absorption band intensity map of slice hair sample.

BL7U

Direct Measurements of Metallic Property of Organic Materials upon Temperature-Dependent Photoelectron Spectroscopy

X. Liu[1], J. P. Yang[2], K. Tanaka[3], H. Tang[4], F. Huang[4], S. Kera[3] and M. Fahlman[1]

[1]*Laboratory of Organic Electronics, ITN, Linköping University, Norrköping SE-60174, Sweden*

[2]*College of Physical Science and Technology, Yangzhou University, Jiangsu 225009, China*

[3]*UVSOR Synchrotron Facility, Institute for Molecular Science, Okazaki 444-8585, Japan*

[4]*Institute of Polymer Optoelectronic Materials and Devices, State Key Laboratory of Luminescent Materials and Devices, South China University of Technology (SCUT), Guangzhou, China*

Engineering electronic properties of pi-conjugated polymers upon functional groups from material synthesis to post-treatment with external dopants is of vital importance for the development of air stable, soluble, effective charge transport materials on organic devices [1]. Doping induced delocalization of (bi) polarons and their intra-chain carrier transport in pi-conjugated polymers is the basis of the field of "organic synthetic metals", as well as the foundation of modern organic electronic devices. For instance, PEDOT:PSS, are commercially available hole-dominant (p-type doping) materials with conductivity up to several thousand S/cm, which can be labelled as semi-metallic polymer [2] with no energy gap and very low density of states (like tail states) at the Fermi level due to the contribution of high (bi)polaron density. The information related to the high-conducting n-type (electron-dominant) ones is rather less, e.g., there is still controversy about the new states near the Fermi level of K-doped picene [3], related to the semiconductor-metal transition. Recently, the successful synthesis of air-stable, soluble, and high conducting n-type polymer PBFDO ($(C_{10}O_4H_4)_n$, shown in the inset of Fig. 1(b)) shows the electron conductivity up to 2000 S/cm and very deep LUMO (lowest unoccupied molecular orbitals) [4]. It is believed that the PBFDO is at the critical regime of Mott transition by n-type self-doping with 0.9 electron per unit during polymerization process while the presence of protons in the solvent was used to balance the negative charge. We carried out a UPS study of our-synthesized PBFDO film, a clear Fermi edge feature on free-standing PBFDO films was obviously visible with a work function of up to 5.4 eV, like clean Pt or Au metals.

Any information related to clear Fermi edge feature in high-conducting organic synthetic metals from photoelectron spectroscopy will offer solid evidence of their metallic properties, but it is missing yet for PBFDO. The temperature-dependent Fermi edge features can provide a test about applying Tomonaga–Luttinger liquid or Fermi liquid/glass theory to electronic transport properties of organic synthetic metals.

In this study, we examined the valence band feature of PBFDO close to the Fermi edge regions using high-resolution photoelectron spectroscopy at UVSOR-III BL7U. We used variable excitation photon energy from 7 to 40 eV and the photoelectron spectra were collected by an electron analyzer (A-1, MB-Scientific) with PBFDO sample at temperature from 10 to 298 K.

Figure 1 (a) and (b) show the valence band feature of PBFDO at 298 and 10 K compared to that of Au. It clearly demonstrates the metallic properties of PBFDO with metal-like Fermi edge. The valence feature at around 0.25 eV of PBFDO might be related to the filled LUMO, which results in a broad spectral feature crossing the Fermi edge as the lower part can be deconvoluted with metallic Fermi-Dirac function. Since there is short of theoretical analysis of the metallic properties of PBFDO, we may tentatively analyze the feature with the convolution of a gaussian valence peak at 0. 25 eV and metallic Fermi edge at 0 eV. Furthermore, Figure 1 (c) and (d) show the temperature dependent feature at 0 eV in PBDFO is very similar to that of Au metal. The broadening of the feature above the 0 eV monotonically increases with temperature. Based on our knowledge, the result is the first direct observation of the metallic Fermi feature in organic materials.

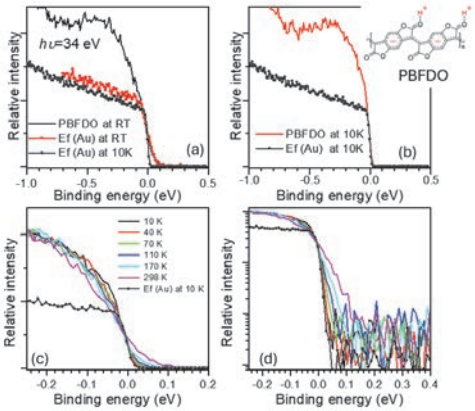

Fig. 1. Valence band feature of PBFDO at photon energy of 34 eV. (a,b) Comparison of Fermi edge feature of PBFDO and Au at 298 and 10 K. (c,d) Fermi edge feature of PBFDO as a function of temperature with linear (c) and logarithmic (d) intensity plots.

[1] A. Heeger, Angew. Chem. Int. Ed. **40** (2001) 2591.
[2] O. Bubnova *et al.,* Nat. Mater. **13** (2014) 190.
[3] A. Ruff *et al.,* Phys. Rev. Lett. **110** (2013) 216403.
[4] H. Tang *et al.*, Nature **611** (2022) 271.

BL7U

Coexistence of Ferromagnetism and Altermagnetism in MnTe Thin Films

R. Akiyama[1], T. T. Sasaki[2], M. Valvidares[3], T. Okauchi[4], K. Tanaka[5], S. Ichinokura[1,2], S. V. Ereemev[6], M. M. Otrokov[7], E. V. Chulkov[8], A. Hariki[4] and T. Hirahara[1]

[1]*Department of Physics, Institute of Science Tokyo, Tokyo 152-8551, Japan*
[2]*National Institute for Materials Science, Tsukuba 305-0047, Japan*
[3]*ALBA Synchrotron Light Source, E-08290 Cerdanyola del Valles, Spain*
[4]*Department of Physics and Electronics, Osaka Metropolitan University, Osaka 599-8531, Japan*
[5]*UVSOR III Synchrotron, Institute for Molecular Science, Okazaki 444-8585, Japan*
[6]*Institute of Strength Physics and Materials Science, Tomsk 634055, Russia*
[7]*Instituto de Nanociencia y Materiales de Aragón (INMA), Zaragoza 50009, Spain*
[8]*Donostia International Physics Center (DIPC), Basque Country, Spain*

Altermagnetic materials exhibit spin-compensated magnetic order like antiferromagnets while breaking time-reversal symmetry like ferromagnets [1]. MnTe, which has a NiAs-type structure, has been identified as an altermagnet with in-plane magnetic moments, as evidenced by nodal spin splitting observed in angle-resolved photoemission spectroscopy (ARPES) [2] and oscillatory x-ray magnetic circular dichroism (XMCD) signals [3]. In our previous study, we demonstrated that embedding 4 layers of MnTe into a topological insulator Bi_2Te_3 (BT) results in the formation of a $Mn_4Bi_2Te_7$/BT heterostructure, where the MnTe layers adjacent to the BT interface adopt a NaCl-type structure and the system exhibits out-of-plane ferromagnetism [4]. Building up on these findings, we consider embedding multilayer MnTe into the minimal unit of BT, a single quintuple layer (1QL- BT), which should allow the growth of MnTe thin films with surfaces and substrate interfaces terminated by Bi and Te atomic layers. However, the influence of such termination modifications on the altermagnetic properties of MnTe thin films remains unclear and requires investigation. Therefore in this study, we fabricated MnTe thin films terminated with Bi and Te atomic layers both at the surface and the interface to the Si substrate and compared their electronic structure with that of pure MnTe films directly grown on Si. Temperature and photon energy dependent *in situ* ARPES measurements were conducted at UVSOR BL-7U with p-polarized photons on and off the nodal plane. The energy and angular resolutions were 15 meV and 0.25°, respectively.

Scanning transmission electron microscopy (STEM) revealed that while these MnTe films terminated with Bi and Te predominantly exhibit the NiAs-type structure, NaCl-type stacking appears near the Si interface, resembling our previously reported $Mn_4Bi_2T_7$/BT heterostructure. XMCD measurements performed at BL29 BOREAS at ALBA confirmed the coexistence of altermagnetic and out-of-plane ferromagnetic signals, reproduced by ab inito calculations. This was also confirmed from ARPES measurements, as shown in Fig. 1. Upon cooling, the nodal splitting emerges in association with the altermagnetic transition (red arrow) at the nodal plane. Furthermore, an exchange splitting at the Γ point, likely induced by ferromagnetism, was also observed by further cooling as shown by the yellow arrow. In contrast, although the nodal splitting was observed for the pure MnTe film grown on Si, the exchange splitting was absent. This was consistent with the XMCD measurement. These findings indicate that the structural change at the interface cants the magnetic moment to the out-of-plane direction, resulting in the coexistence of altermagnetism and ferromagnetism in the MnTe films with Bi and Te termination.

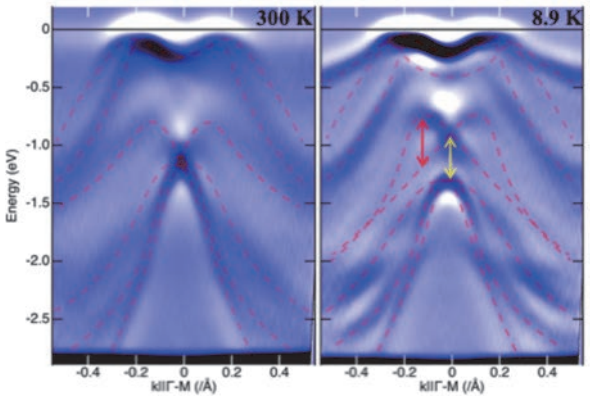

Fig. 1. Band structure of MnTe terminated with Bi and Te, measured along the Γ-M direction measured with hν = 19 eV. The left panel shows the paramagnetic state measured at T = 300 K and the right one shows the coexistence of altermagnetic and ferromagnetic states measured at T = 8.9 K. Red and yellow arrows indicate altermagnetic and ferromagnetic band splitting, respectively.

[1] L. Šmejkal *et al.*, Phys. Rev. X **12** (2022) 031042.
[2] S. Lee *et al.*, Phys. Rev. Lett. **132** (2024) 036702.
[3] A. Hariki *et al.*, Phys. Rev. Lett. **132** (2024) 176701.
[4] T. Hirahara *et al.*, Nat Commun. **11** (2020) 4821.

UVSOR User 6

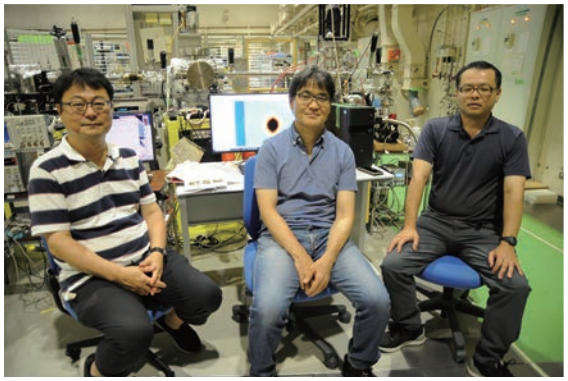

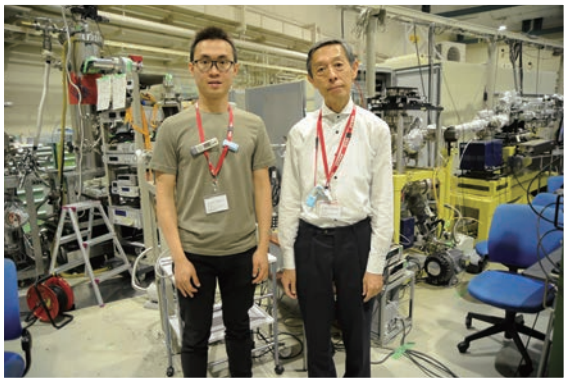

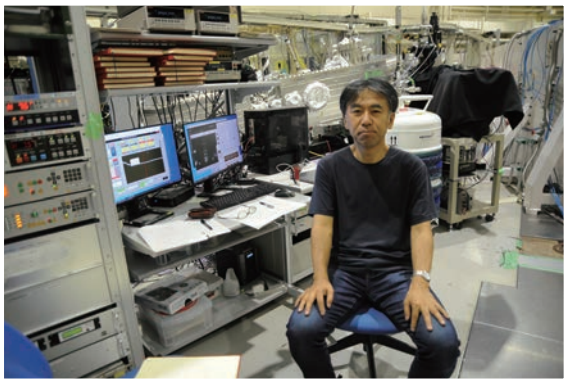

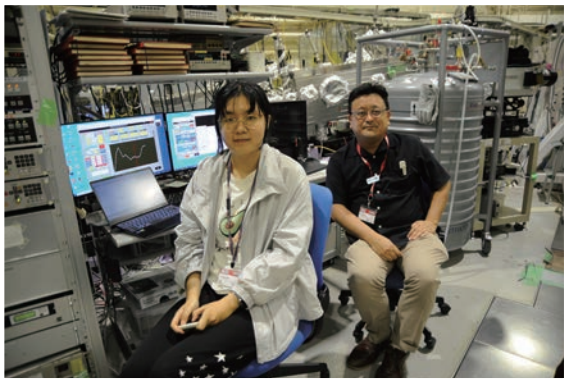

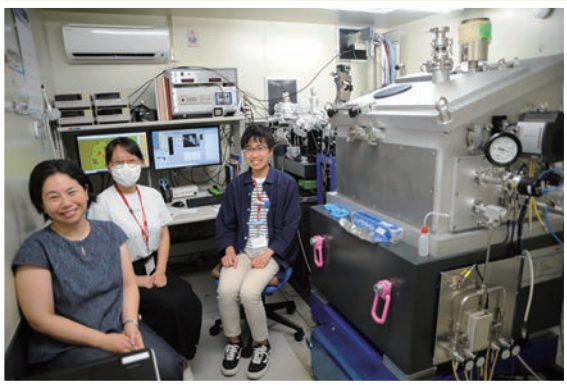

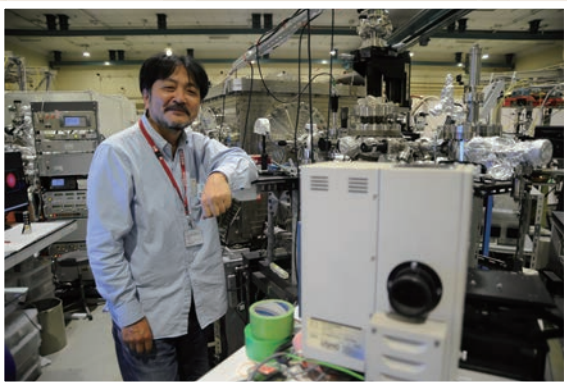

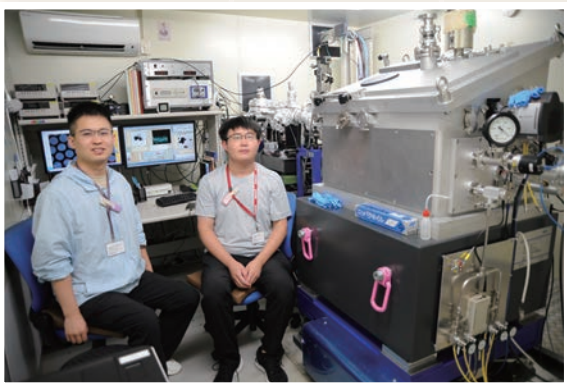

UVSOR User 7